Bio-Design and Manufacturing (2020) 3:98–108
https://doi.org/10.1007/s42242-020-00066-8

RESEARCH ARTICLE

A new design of 3D-printed orthopedic bone plates with auxetic structures to mitigate stress shielding and improve intra-operative bending

Sanjairaj Vijayavenkataraman[1,2] · Akhil Gopinath[3] · Wen F. Lu[3]

Received: 5 January 2020 / Accepted: 20 February 2020 / Published online: 19 March 2020

Abstract
Orthopedic bone plates are most commonly used for bone fracture fixation for more than 100 years. The bone plate design had evolved over time overcoming many challenges such as insufficient strength and excessive plate–bone contact affecting the blood circulation. However, it is only made of two materials, either stainless steel (AISI 316L) or titanium (Ti–6Al–4V). There are two main limitations of metallic bone implants, namely stress shielding and the problem of malocclusion caused by the displacement of the fracture site during healing. To overcome the two problems, a new bone plate design with the incorporation of auxetic structures is proposed in this work. This study aims to use auxetic structure section in the bone plate that would decrease the stiffness of the region, thereby mitigating the stress-shielding effect and at the same time act as a deformable section to enable intra-operative bending for effective alignment while having enough bending strength and stiffness. Two different auxetic structures namely re-entrant honeycomb and missing rib structures were considered. The auxetic structure incorporated bone plates were designed, finite element analysis was done, fabricated using direct metal laser sintering technique, and tested. The results indicate that the re-entrant honeycomb structure incorporated bone plates serve as an effective bone design compared to the conventional bone plate design, in terms of stress shielding and intra-operative bending while offering similar mechanical and bending strength.

Keywords Bone plates · Negative Poisson's ratio structures · 3D printing · Additive manufacturing · Stress shielding

Introduction

Orthopedic bone plates are most commonly used for bone fracture fixation among the other internal fixation methods such as by wires, nails, rods, pins, and screws, due to its excellent resistance to compression, tension, bending, shearing, and other rotational forces [1]. For more than 100 years, bone plates have been used for fracture (internal) fixation. The first bone plate introduced by Lane [2] in 1895 failed due to corrosion problems. Bone plates with increased corrosion resistance were then introduced by Lambotte [3] and Sherman [4], which also failed due to their insufficient strength. An improved design was introduced by Eggers [5] but still failed due to insufficient strength. In 1949, Danis [6] proposed a compression plating called coapteur which had a side screw that is tightened to suppress the interfragmentary motion and lead to increased stability. Danis's design was found to result in primary bone healing and inspired all the subsequent bone plate designs till now. Many improvements were suggested from then, including introduction of oval holes for screw tightening for interfragmentary compression [7], and design with a temporary tensioner [8], which eventually led to the dynamic compression plate (DCP) design in 1967 [7].

DCP possessed several advantages compared to the earlier designs and was widely adopted but there were certain limitations. Cortical necrosis occurred as a result of excessive plate–bone contact leading to disturbed periosteal blood circulation [9]. To overcome this limitation, an improved design with reduced plate–bone contact called limited contact-

✉ Sanjairaj Vijayavenkataraman
vs89@nyu.edu

1 Division of Engineering, New York University Abu Dhabi, Abu Dhabi, UAE

2 Department of Mechanical and Aerospace Engineering, Tandon School of Engineering, New York University, Brooklyn, NY, USA

3 Department of Mechanical Engineering, National University of Singapore (NUS), Singapore, Singapore

dynamic compression plate (LC-DCP) was introduced by Gautier and Perren [10]. Although the inventors claimed that LC-DCP design reduced the plate–bone contact by 50% and prevented cortical necrosis [10], further studies by Field et al. [11] showed no apparent differences in the interface contact area and Jain et al. [12] concluded there is no difference in the measured cortical blood flow. Hence, another design called point contact fixator (PC-Fix) was introduced with a conical connection between screw heads and screw holes [13]. Further, the "less invasive stabilization system" (LISS) design was proposed where the plate was fixed to the bone with unicortical screws [14]. Finally, in 2000, both the PC-Fix and LISS designs were incorporated, and the locking compression plate (LCP) design was introduced. LCP has the provision to use either conventional cortex screws or conical contact screws and thus can be used in three ways including conventional LCP, pure internal fixator (PIF), or a combination of both [15].

LCP is the most commonly used bone plate design, and despite its advantages, it is only made of two materials, either stainless steel (AISI 316L) or titanium (Ti–6Al–4V) [16]. Although many other non-metallic materials were reported in the literature for use as orthopedic implant material, they suffer from many limitations. Polymers such as polylactic acid (PLA), polyglycolic acid (PGA), polymethylmethacrylate (PMMA), polyhydroxybutyrate (PHB), polycaprolactone (PCL), polydioxanone (PDS), polyether ether ketone (PEEK), and poly(2-hydroxy-ethyl methacrylate) (PHEMA) are biocompatible and can be used as implant materials [17, 18]. However, these polymers possess weak mechanical properties and can be used only as dental implants and they are not suitable for orthopedic bone plate application [19, 20]. Bioactive ceramics such as alumina and zirconia, though having appreciable mechanical properties compared to polymers, are still weaker compared to the native bone in terms of tensile strength and fracture toughness, thus preventing its usage in high load-bearing applications such as bone plates [21]. Due to these reasons, metallic bone plates made of stainless steel and titanium (Ti) are the most widely used.

There are two main limitations of metallic bone implants. Firstly, stress shielding is a common problem associated with metallic bone plates [22]. Given the constraints with materials, the problem could only be overcome by improving the bone plate structural design. Not many works were reported on this subject. Pobloth et al. [23] used 3D porous Ti-meshed structures at the point of defect to minimize stress shielding while ensuring resistance against mechanical failure. The stiffness and porosity of the mesh structure were controlled by varying the strut thickness. In vivo studies proved that the less stiff structures resulted in enhanced bone regeneration. However, this study only dealt with Ti-meshed scaffolds for bone tissue regeneration and not bone plates for fracture fixation. The second limitation is the problem of malocclusion caused by displacement of the fracture site during healing [24]. This is due to the inability of the surgeon to visually align the segments of the bone and affix a metal plate, as the commercial bone plates come with only certain standard shapes and sizes. Cervantes et al. [25] reported a modified bone plate design with a deformable section to give surgeons the ability to reduce misalignments at the fracture site by intra-operative bending. However, the bending strength and stiffness of the proposed design was relatively lower for the deformed plate.

Auxetic structures exhibit a negative Poisson's ratio (NPR) (i.e.,) they expand on stretching and contract on compression. In other words, NPR is defined as the ratio of transversal expansion to the axial compression. Due to this special property, these structures are being investigated for use in biomedical implants and medical devices [26]. Although use of auxetic structures in bone plates and implants exist conceptually since long, the reported works on design and fabrication of such implants are few. In a recent study [27], a combination of negative and positive Poisson's ratio structures was used to design meta-implants to prevent retraction and implant loosening under biomechanical loading. This study [27] specifically focused on the femoral part of the total hip replacement (THR) implant and is not designed for incorporation in the bone plates which are at a different scale. Mehmood et al. [28] fabricated polyurethane-based auxetic bone plates with a NPR value ranging between -0.68 and -0.87 to render the micro-movement of the bone plates as that of the natural bone. The study has been done on polymeric materials while metallic bone plates are preferred due to their long-term stability.

In this study, auxetic or negative Poisson's ratio (NPR) structures are introduced in the metallic bone plates as an effective solution to the above problems. This study aims to use auxetic structure section in the bone plate that would decrease the stiffness of the region, thereby mitigating the stress-shielding effect and at the same time act as a deformable section to enable intra-operative bending for effective alignment while having enough bending strength and stiffness.

Experimental section

Design and finite element analysis (FEA) of Re-entrant Honeycomb auxetic structures

SolidWorks 2016 is used for modeling, and ABAQUS (Version 6.13) is used for FEA. Re-entrant honeycomb and missing rib structures are considered in this work due to their high anisotropy like the native bone and their versatility in terms of the mechanical properties they could achieve

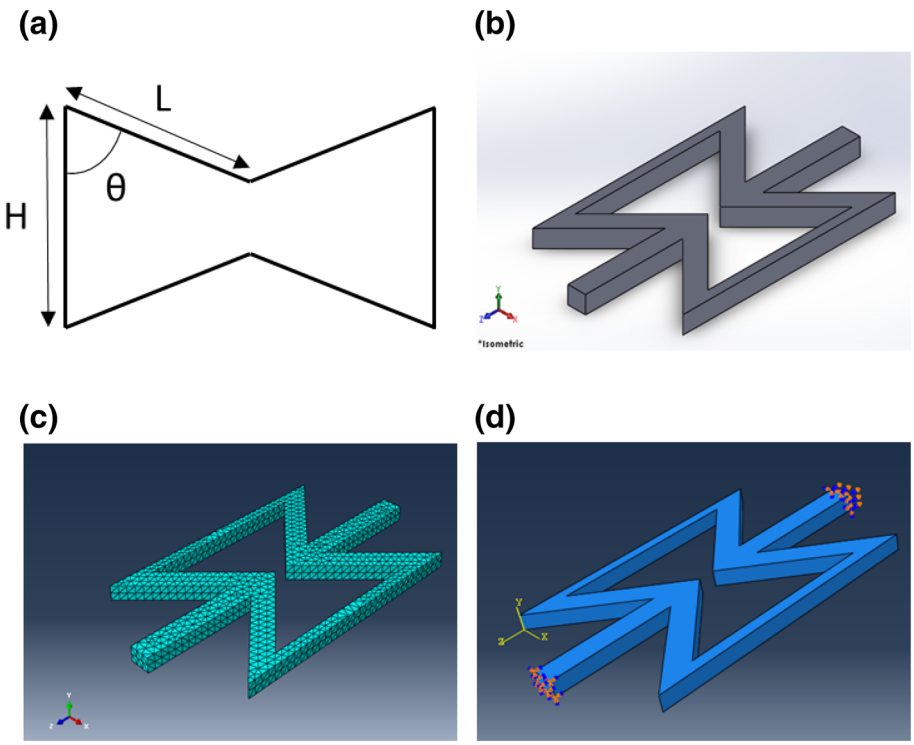

Fig. 1 **a** A representative 2D unit cell of the re-entrant honeycomb NPR structure, **b**, **c** CAD model (solid works) and meshed image (ABAQUS) of a 3D unit cell of the re-entrant honeycomb NPR structure with dimensions $H = 12$ mm, $L = 6$ mm and $\theta = 45°$, **d** boundary conditions applied to the re-entrant honeycomb unit cell structure

[27, 29]. Figure 1a shows a 2D unit cell of the re-entrant honeycomb NPR structure. Three basic parameters define a re-entrant honeycomb structure, namely base length (H), rib length (L), and inclination angle (IA), θ. A 3D re-entrant honeycomb NPR structure is shown in Fig. 1b, and the meshed 3D structure is shown in Fig. 1c. FEA was performed to calculate the NPR values of the auxetic structures at different H, L, and θ. For analysis, the member perpendicular to the base length, in the $+z$-direction, was constrained, and displacement (20% strain) was applied to the opposite member, in the $-z$-direction, as shown in Fig. 1d.

Under tensile or compressive loading, the re-entrant struts, i.e., the length L undergo bending whereas the vertical struts with length H undergo axial deformation. Yang et al. [30] derived an analytical model for re-entrant honeycomb structure as below:

$$v = -\frac{L^2 \cos\theta(\alpha - \cos\theta)}{2\alpha t^2 + L^2 \sin\theta^2} \tag{1}$$

where v Poisson's ratio, α H/L, and t strut thickness.

The Taguchi method was employed for the design of experiments (DOE). Taguchi method uses a set of arrays called orthogonal arrays containing the minimum number of experiments, which will depict the effect of performance parameters on a response parameter. In our case, H, L, and θ are the performance parameters and Poisson's ratio from FEA is our response parameter. Three performance parameters with four levels each resulted in 16 combinations (shown in Table 2). A strut thickness of 50 μm is used. The data were analyzed using MINITAB software to study the influence of each parameter on Poisson's ratio.

Based on the DOE, a unit cell was chosen for to study the effect of number of unit cells and the number of layers on the NPR value. For studying the effect of the number of layers on the NPR value, a vertical rib of 50 μm square cross-section was used to join the subsequent layers. The magnitude of reaction force was calculated for 20% strain applied, and Young's modulus was calculated using the formula:

$$E = \frac{FL}{A\Delta L} \tag{2}$$

where E Young's modulus, F reaction force, A cross-sectional area, and ΔL strain applied.

Porosity was calculated by the formula:

$$\text{Porosity} = \left(1 - \frac{V_{\text{scaffold}}}{V_{\text{cube}}}\right) * 100 \tag{3}$$

where V_{scaffold} is the volume of the designed scaffold and V_{cube} is the volume of the cube enclosing the outer dimensions of the scaffold.

Design and finite element analysis (FEA) of missing rib auxetic structures

Missing rib structures are formed when ribs are removed selectively from the intact structure. The angles α and β, and

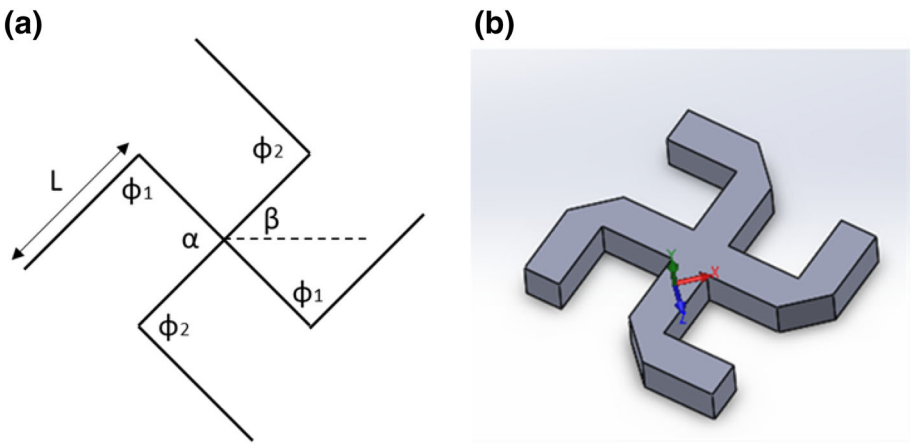

Fig. 2 **a** A representative 2D unit cell of missing rib NPR structure, and **b** CAD model (Solid works) of a 3D unit cell of the missing rib NPR structure with ϕ_1 and $\phi_2 = 90°$ and, $\beta = \alpha/2$

the strut length (L) define this structure, as shown in Fig. 2a. The angle between the struts, ϕ_1 and ϕ_2, is kept at 90° and to maintain symmetry, $\beta = \alpha/2$.

FEA was performed per the same procedure stated above for the re-entrant structure. An analytical model developed by Smith et al. [31] to evaluate the NPR of missing rib structures was used to calculate the theoretical PR:

$$v = -\tan\beta \tan(\alpha - \beta). \tag{4}$$

Computation of NPR from the FEA

FEA was performed on both the re-entrant and missing rib auxetic structures as mentioned in the previous sections. For analysis, the member perpendicular to the base length, in the $+z$-direction, was constrained, and displacement (20% strain) was applied to the opposite member, in the $-z$-direction, as shown in Fig. 1d. To calculate Poisson's ratios, we evaluated the transverse elastic deformation of the unit cell resulting from axial strains. Poisson's ratio at each of the nodes on the side edges was calculated using the below equation:

$$v = -\frac{\varepsilon_{xx}}{\varepsilon_{zz}} \tag{5}$$

The average of Poisson's ratio of all the nodes was computed and taken as the NPR of the unit cell.

Design and finite element analysis (FEA) of bone plates

SolidWorks 2016 was used to model the bone plates. The properties of stainless steel 316L were used for FEA. The thickness of the bone plate is 3.6 mm, and the width is 13.05 mm, with 6 screw holes, in line with the standard commercial bone plate sizes. Six screw holes were designed with 16 mm spacing between the holes. The design specifications are summarized in Table 1. To determine the best position of the auxetic structure on the bone plate and evaluate the stress distribution under loading, FEA was done for four different models, control (without any auxetic structure), and with re-entrant auxetic sections at the center, position P1, and position P2 (shown in Fig. 7).

Table 1 Technical specifications of bone plate

Type of bone plate	Compression
Material of bone plate	Stainless steel
No. of holes	6
Width of bone plate	13.05 mm
Thickness of bone plate	3.6 mm
Bone screw diameter	4.5 mm

3D printing of bone plates

Three bone plate models were designed with the specifications given in Table 2, namely control (without any NPR structure), and bone plates with re-entrant and missing rib NPR structures at the center of the plate and were fabricated using direct metal laser sintering (DMLS) technique with E0S M290. DMLS is a technique which uses laser power to fuse the metal powder particles, layer by layer, to form the 3D structure. The laser type used was ytterbium (Yb) fiber laser of power 400 W. The laser focus diameter was 100 μm. To prevent warping of the structure and to avoid the support structures during printing in the NPR region, the specimens were printed in a 45-degree platform. After printing, the post-processing included wire cutting of the bone plate specimens from the base platform and cleaning the residual powders.

Testing of bone plates

The testing of bone plates was done as per standard ASTM F-32. An INSTRON machine and apparatus were used per the standards shown in Fig. 8d. The bone plate is placed symmetrically so that the loading rollers are aligned between the

Table 2 Taguchi orthogonal DOE for FEA of 3D re-entrant honeycomb NPR structures

IA	*H*	*L*	Analytical Poisson's ratio	FEA Poisson's ratio
60	0.8	0.65	− 0.48	− 0.55
60	0.9	0.6	− 0.65	− 0.72415
60	1	0.54	− 0.87	− 0.98535
60	1.1	0.48	− 1.13	− 0.9747
70	0.8	0.6	− 0.38	− 0.41085
70	0.9	0.54	− 0.50	− 0.50107
70	1	0.48	− 0.65	− 0.74474
70	1.1	0.65	− 0.52	− 0.58188
80	0.8	0.54	− 0.23	− 0.3027
80	0.9	0.48	− 0.30	− 0.288
80	1	0.65	− 0.25	− 0.30452
80	1.1	0.6	− 0.30	− 0.30268
90	0.8	0.48	0.00	0.296
90	0.9	0.65	0.00	0.299
90	1	0.6	0.00	0.295
90	1.1	0.54	0.00	0.327

holes. The center span "a" and the loading span "h" are kept as 35 mm and 23 mm, respectively. The load is applied at a displacement rate of 1 mm/min. The load–displacement graph is derived automatically from the test setup. From the load–displacement curve, the bending stiffness and the proof load was calculated. The bending stiffness (K) was calculated from the maximum slope of the load–displacement graph, and the proof load (P) was calculated from the graph, by drawing a line parallel to the linear portion of the curve at 0.2% offset. The point at which this line meets the load–displacement curve was the proof load. The bone plate structural stiffness, also termed as the flexural rigidity, was calculated using the formula:

$$EI = \frac{(2h + 3a)Kh^2}{12} \tag{6}$$

where E Young's modulus, I second moment of inertia, a center span, h loading span, and K bending stiffness.

Bending strength was calculated using Eq. (6):

$$\text{Bending strength} = \frac{Ph}{2} \tag{7}$$

Fatigue testing (up to 100,000 cycles) per the standards was also performed using the same setup.

Statistical analysis

Experiments were run in triplicates, and all measurements were expressed as mean ± SD. One-way ANOVA test was used to determine any significant differences existed between the mean values of the experimental groups. Differences were considered statistically significant at $p < 0.05$.

Results and discussion

Design and FEA of Re-entrant Honeycomb auxetic structures

A preliminary analysis was performed to evaluate the effect of base length H, rib length L, and inclination angle θ on Poisson's ratio of the structure. Poisson's ratio is also influenced by $\alpha = H/L$ ratio. The unit cell with dimensions $H =$ 12 mm, $L = 6$ mm, and IA = 45° was considered as the control, and each dimension was varied (i.e.,) with $H = 12$ mm, L and IA are varied; with $L = 6$ mm, H and IA are varied, and IA = 45°, H and L are varied.

Effect of base length

The effect of base length on Poisson's ratio of a re-entrant honeycomb structure was studied by keeping the other dimensions constant ($L = 6$ mm, $t = 1$ mm and IA = 45°). The range of base length for the given H/L ratio in our analysis was constrained by two factors: (1) decreasing H below 11.5 mm resulted in overlapping of re-entrant ribs and (2) increasing above 13.5 mm resulted in large errors between FEA and analytical value. In other words, the ratio α should be less than or equal to 2.25 for the relative error to be within 20%. The actual behavior of the scaffolds with $\alpha > 2.25$ needs experimental validation. Base length is varied from 11.5 to 13.5 mm based on the above constraints. The results are shown in Fig. 3a. The NPR values increase with increasing base length.

Effect of rib length

The range of L values is limited to 5.5 to 6 mm due to constraints of α value in FEA, as detailed in "Effect of base length" section. The results are shown in Fig. 3b, and it can be seen that the NPR values decrease as the rib length increases. Bending is more prominent in the structures with shorter ribs, and hence, the NPR value is higher in structure with a shorter rib length.

Effect of inclination angle

Inclination angle is one of the dominant design parameters for a re-entrant honeycomb structure. The minimum angle is constrained by H and L and the overlapping of the re-entrant structures. The effect of the inclination angle on Poisson's ratio was studied by keeping the other dimensions constant

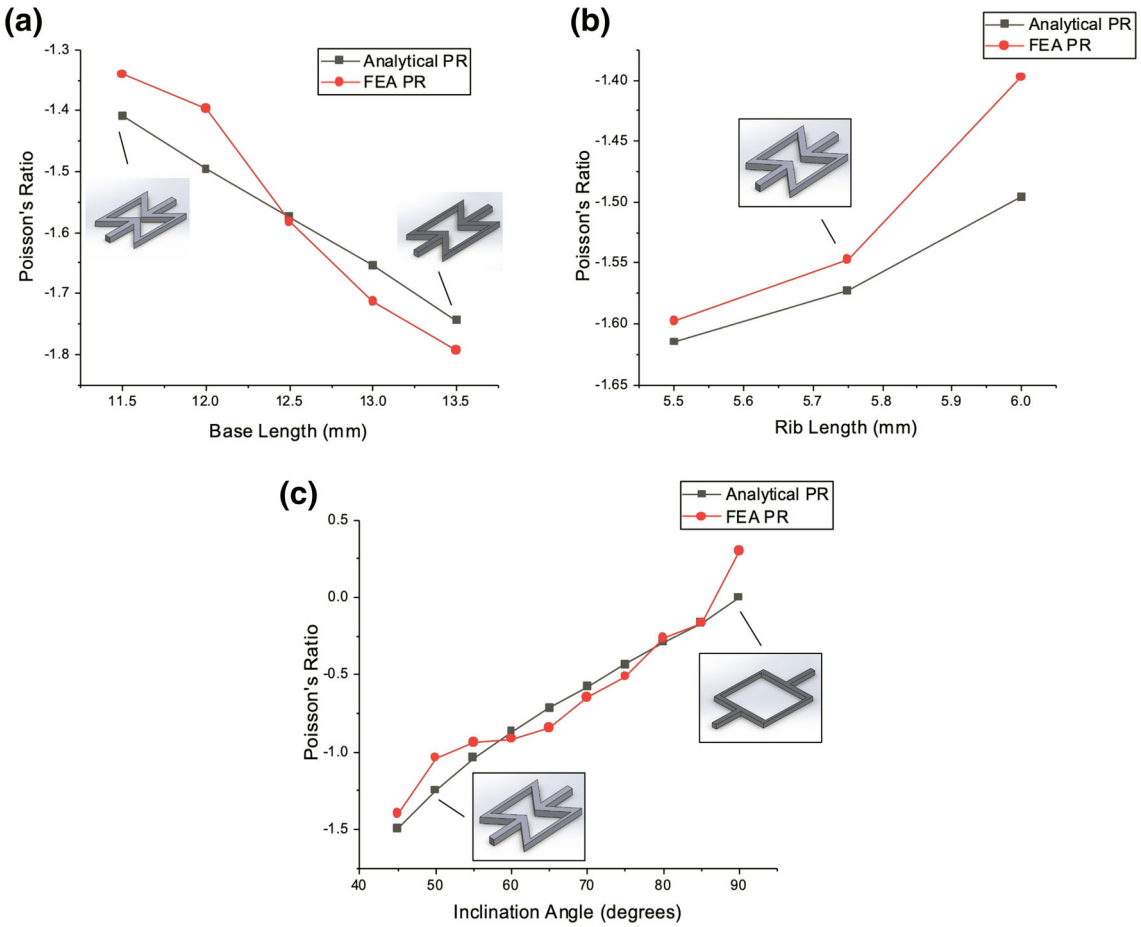

Fig. 3 **a** Effect of base length on PR, **b** Effect of rib length on PR, and **c** Effect of inclination angle on PR of the re-entrant auxetic structure

($H=$ 12 mm, $L=$ 6 mm, and $t=$ 1 mm), and the inclination angle varied from 45° to 90°. The results are shown in Fig. 3c. The NPR value decreases with increasing IA. The more inward the re-entrant strut is, the more pronounced is the auxetic behavior. At higher inclination angles, the flexure of the rib length strut decreases. On reaching 90°, the structure starts showing positive PR behavior and exhibits a PR closer to that of the PR of the material, irrespective of the dimensions of H and L. This contrasts with the value predicted by the analytical formula at 90°. Representative images of the CAD model, stress and strain contours for IA values of 50° and 90° are shown in Fig. 4.

Taguchi DOE for auxetic structures in the bone plate

In the preliminary studies ("Effect of base length"–"Effect of inclination angle" sections), the effect of various dimensions on the PR of the re-entrant honeycomb unit cell was studied. Taking this study as a base, the operating ranges of H, L, and θ for bone plate sections were chosen, keeping in mind the technical specifications of bone plates. The Taguchi method was employed for the design of experiments (DOE). The 3 performance parameters (H, L, and θ) and 4 levels in each resulted in 16 combinations as shown in Table 2. While the PR values calculated by analytical and FEA methods matched closely for most of the cases, the PR values differ significantly when IA is 90°. At IA = 90°, the structure starts showing positive PR behavior and exhibits a PR closer to that of the PR of the material, irrespective of the dimensions of H and L. But the analytical value is zero due to the limitations of the analytical model.

The response data were analyzed in MINITAB 18, which ranked the effect of the 3 performance parameters on the PR, as shown in Table 3. As evident from our preliminary analysis, the ranking of parameters was in the order IA, H, and L. The IA has the most prominent effect on the PR of the auxetic structure. Hence, scaling up or down the H and L values do not contribute much in terms of PR variation.

Based on the DOE, the auxetic structure with $H=0.8$ mm, $L=0.6$ mm, $t=1$ mm, and IA = 70° was chosen as the unit cell structure. Also, the PR range of this specimen lies between 0.35 and 0.5, which is the clinical range preferred for tissue engineering scaffolds [32–35]. It is to be noted that this

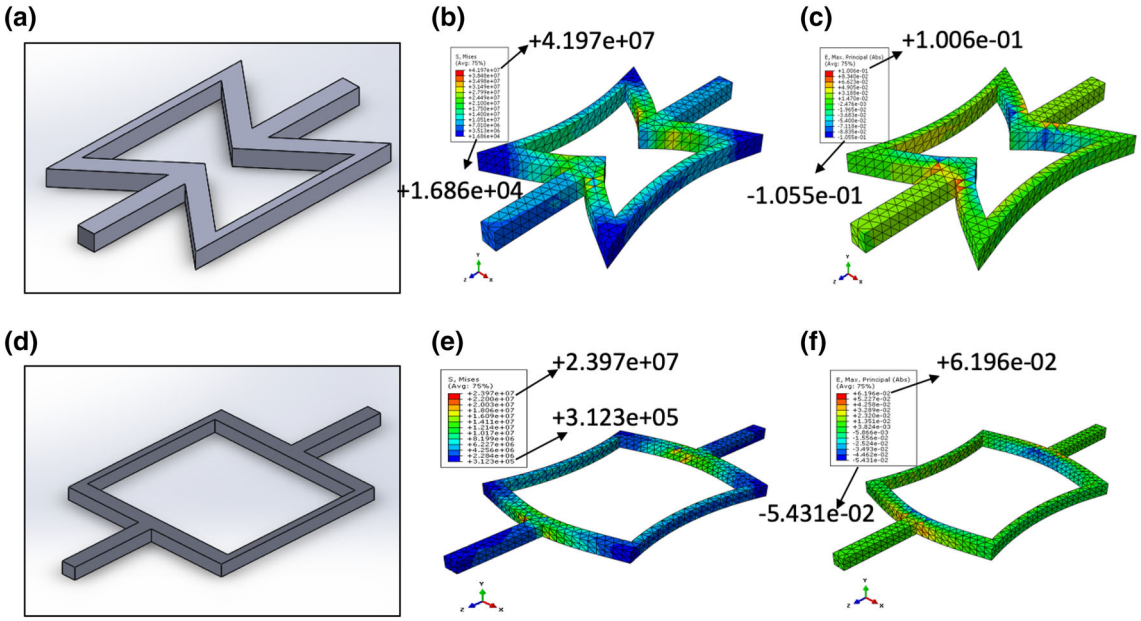

Fig. 4 **a–c** CAD model, stress contour (units: Pa) and strain contour, respectively, of the re-entrant honeycomb auxetic structure with IA = 50°, and **d–f** CAD model, stress contour and strain contour, respectively, of the re-entrant honeycomb auxetic structure with IA = 90°

Table 3 Ranking of performance parameters from MINITAB

Level	IA	*H*	*L*
1	− 0.8085	− 0.2419	− 0.4279
2	− 0.5596	− 0.3036	− 0.3655
3	− 0.2995	− 0.4349	− 0.2857
4	0.3042	− 0.3831	− 0.2843
Delta	1.1128	0.1930	0.1435
Rank	1	2	3

PR range is based on only a few published studies [32–35]; however, verification of this claim and measurement of Poisson's ratio of actual biological materials/tissues remains a challenge [35, 36].

Effect of number of unit cells and number of layers

The effect of increasing unit cells (biaxial) and the number of layers on the mechanical properties of the auxetic structure was also studied. The number of unit cells was increased from a 3 × 3 matrix to a 13 × 13 matrix. However, increasing the number of unit cells yielded no significant variation in Young's modulus. Similarly, increasing the number of layers from 1–8 also did not result in much variation of Young's modulus and porosity of the structure. A representative 3D re-entrant honeycomb auxetic structure with 6 layers and 3 × 3 matrix is shown in Fig. 5.

Design and FEA of missing rib auxetic structures

The angle α is the dominant performance parameter in the missing rib structure. The angle was varied from 30° to 70°, and the PR was determined. The results are shown in Fig. 6a. The analytical values calculated from Smith's model [31] differ much with the PR value determined through FEA as seen in Fig. 6a, due to the shortcomings of Smith's model (it does not consider the angular deformation in determining the PR). Also, similar to the re-entrant honeycomb structure, the number of unit cells and the number of layers did not have any significant effect on Young's modulus and porosity of the missing rib structure. A representative 3D missing rib auxetic structure with 6 layers and 3 × 3 matrix is shown in Fig. 6b.

Design and finite element analysis (FEA) of bone plates

To determine the best position of the auxetic structure on the bone plate, FEA was performed on four different models, control (without any auxetic structure), and with re-entrant auxetic sections at the center, position P1, and position P2, as shown in Fig. 7. The position closer to the center is termed P1 and that away from center is termed P2. The bone plate specifications and details are explained in the experimental section.

The reaction force and stress values were recorded. The reaction force developed in the control specimen is 65% higher than the specimen with auxetic section at the cen-

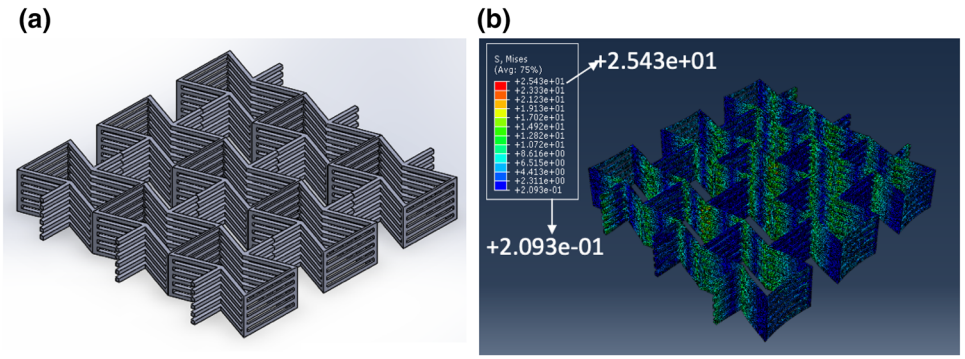

Fig. 5 **a**, **b** CAD model and stress contour (units: Pa) of a representative 3D re-entrant honeycomb auxetic structure with 6 layers and 3 × 3 matrix

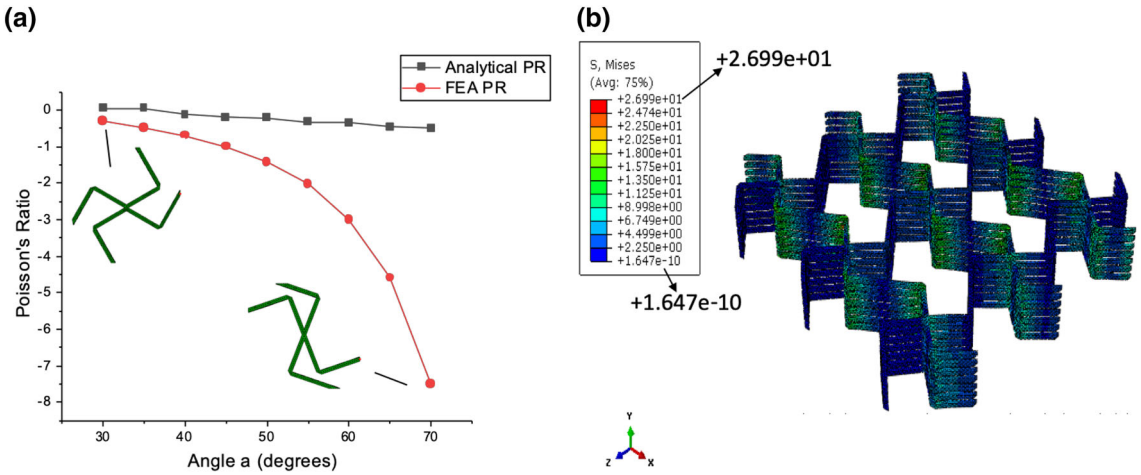

Fig. 6 **a** Effect of angle α on PR and **b** stress contour (units: Pa) of a representative 3D missing rib auxetic structure with 6 layers and 3 × 3 matrix

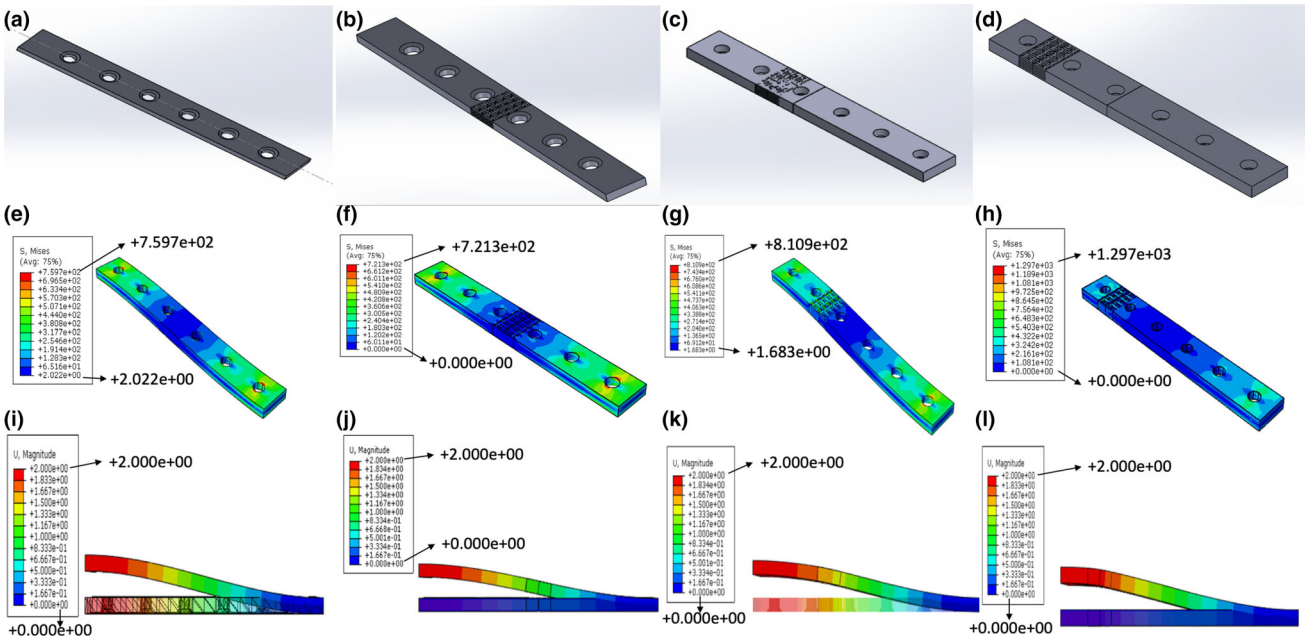

Fig. 7 CAD Model, stress contour (units: Pa), and displacement contour, respectively, of 4 bone plates **a**, **e**, **i** control (without any auxetic structure), **b**, **f**, **j** re-entrant auxetic sections at the center, **c**, **g**, **k** re-entrant auxetic sections at position P1, and **d**, **h**, **l** re-entrant auxetic sections at position P2

Table 4 Reaction force and maximum stress values with auxetic sections at different positions of the bone plates

	Control	Auxetic section at center	Auxetic section at P1	Auxetic section at P2
Reaction force (N)	725.8	251.8	264.6	370.4
Max. stress (MPa)	759	721	810.9	1297.3

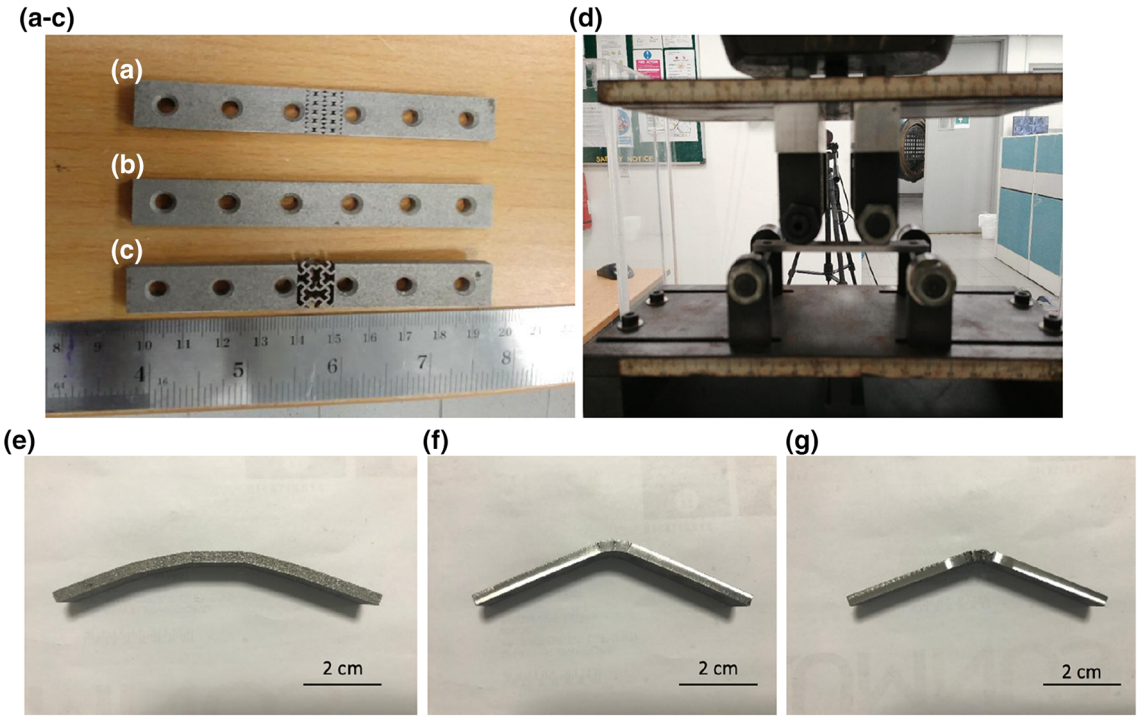

Fig. 8 3D-printed bone plates **a** with re-entrant honeycomb auxetic structure at the center, **b** control (without any auxetic structure), **c** with missing rib auxetic structure at the center, **d** 4 point bending test setup used for testing of bone plates, bending contour of **e** control (without any auxetic structure), **f** bone plate with re-entrant honeycomb auxetic structure at the center, and **g** bone plate with missing rib auxetic structure at the center

ter. Comparing the auxetic sections at different positions, the one closer to the point of load application was found to have higher stress levels and higher reaction force. The reaction force developed was lower with auxetic sections at P1 and P2, compared to the control but the stress levels are comparatively higher and could be a concern from a bone healing perspective. The values are tabulated in Table 4. The displacement and stress contours of the four different designs are shown in Fig. 7.

3D printing of bone plates

From the FEA results, the auxetic structure placed at the center of the bone plate was better than the control and the other positions P1 and P2. Hence, three bone plate models were designed with the specifications given in Table 2, namely control (without any NPR structure), and bone plates with re-entrant and missing rib NPR structures at the center of the plate and were fabricated using DMLS method, shown in Fig. 8a–c.

Testing of bone plates

The testing of bone plates was done as per standard ASTM F-32. The results are shown in Table 5. Bending stiffness is the resistance to deformation while bending strength is resistance to fracture. The bending stiffness is found to be lower in bone plates with the auxetic structure section. The mean value of bending stiffness is found to be 491.28 ± 59 N/mm for control bone plate, 54.40 ± 5.3 N/mm for re-entrant, and 38.03 ± 6 N/mm for missing rib structures. One of the aims of introducing the auxetic structure is to lower the bending stiffness to have a deformable section to enable intra-operative bending for effective alignment while having enough bending stiffness to resist deformation. Bending strength of the re-entrant honeycomb structure incorporated bone plate is 11.26 ± 0.95 Nm, which is a little higher than the control

Table 5 Results of the bending and fatigue testing of the bone plates

	Control	Re-entrant honeycomb	Missing rib
Bending stiffness, K (N/mm)	491.29 ± 59	54.40 ± 5.3	38.03 ± 6
Flexural rigidity, EI (N/mm^2)	3.27 ± 0.39	0.36 ± 0.03	0.25 ± 0.04
Proof load, *P* (N)	963.28 ± 54	979.06 ± 83	79.44 ± 7
Bending strength (Nm)	11.08 ± 0.63	11.26 ± 0.95	0.91 ± 0.08
Fatigue (no. of cycles)	100,000	100,000	8342 ± 732

specimen (11.08 ± 0.63 Nm), while the missing rib structure incorporated bone plate has the lowest bending strength of 0.91 ± 0.08 Nm. Bending strength is directly proportional to the proof load, and consequently, the re-entrant honeycomb structure incorporated bone plate has higher bending strength than the control specimen. Also, both the control specimen and the re-entrant honeycomb structure incorporated bone plate endured 100,000 cycles of loading in the fatigue testing per the bone plate requirements, while the missing rib honeycomb structure incorporated bone plate failed before reaching 9000 cycles. The contour of the specimens after the bending tests is shown in Fig. 8e–g. The bending contour of the auxetic structure incorporated bone plate is smoother compared to the control specimen.

Conclusion

Auxetic structures incorporated orthopedic bone plates were additively manufactured and tested in this study. The introduction of the auxetic structure reduces the stiffness (and hence expected to reduce the stress-shielding effect) and also acts as a deformable section to enable intra-operative bending for effective alignment during surgery. Of the two different auxetic structures studied, the re-entrant honeycomb structure exhibits more NPR behavior than the missing rib structure and Poisson's ratio of the re-entrant honeycomb structure could be easily tuned based on the application requirements than the missing rib structure. Bone plates with the re-entrant honeycomb structure have higher bending strength and lower bending stiffness than the conventional bone plate design and have a much smoother bending contour. It also sustains the fatigue testing of 100,000 cycles similar to the control specimen, while the bone plates with the missing rib structure fail before reaching 10,000 cycles. The FEA studies show that the maximum stress with the auxetic structure incorporated bone plates is much lower thereby expected to decrease the stress-shielding effect and augment the bone healing process. Also, the optimal position of the auxetic structure is the center of the bone plate, in the region of lowest stress, which reduces the reduction force value by 65%, enabling intra-operative bending during surgery. Thus, incorporation of auxetic structures in the bone plate design might be an effective solution to reduce stress shielding, aid in intra-operative bending, and augment the bone healing process.

Compliance with ethical standards

Conflict of interest The authors declare that there is no conflict of interest.

Ethical Approval This study does not contain any studies with human or animal subjects performed by any of the authors.

References

1. Stiffler KS (2004) Internal fracture fixation. Clin Tech Small Anim Pract 19(3):105–113
2. Bechtol CO, Fergunson AB, Laing PG (1959) Metals and engineering in bone and joint surgery. Medicine. 1:2. https://doi.org/10.1002/bjs.18004720543
3. Lambotte A (1909) Technique et indication des prothèses dans le traitement des fractures. Presse Med 17:321
4. Sherman W (1912) Vanadium steel bone plates and screws. Surg Gynecol Obstet 14:629–634
5. Eggers G, Ainsworth WH, Shindler TO, Pomerat CM (1951) Clinical significance of the contact-compression factor in bone surgery. AMA Arch Surg 62(4):467–474
6. Danis DR (1949) Université de Bruxelles. Théorie et pratique de l'ostéosynthèse: par Robert Danis. Masson (Niort), Paris
7. Bagby GW, Janes JM (1958) The effect of compression on the rate of fracture healing using a special plate. Am J Surg 95(5):761–771
8. Müller ME, Bandi W, Bloch H, Allgöwer M, Willenegger H, Mumenthaler A, Schneider R, Steinemann S, Straumann F, Weber B (2012) Technique of internal fixation of fractures. Springer, Berlin
9. Perren SM, Cordey J, Rahn BA, Gautier E, Schneider E (1988) Early temporary porosis of bone induced by internal fixation implants. A reaction to necrosis, not to stress protection? Clin Orthop Relat Res 232:139–151
10. Gautier E, Perren S (1992) Limited contact dynamic compression plate (LC-DCP)—biomechanical research as basis to new plate design. Der Orthopade 21(1):11–23
11. Field JR, Hearn TC, Caldwell CB (1997) Bone plate fixation: an evaluation of interface contact area and force of the dynamic compression plate (DCP) and the limited contact-dynamic compression plate (LC-DCP) applied to cadaveric bone. J Orthop Trauma 11(5):368–373
12. Jain R, Podworny N, Hupel TM, Weinberg J, Schemitsch EH (1999) Influence of plate design on cortical bone perfusion and fracture healing in canine segmental tibial fractures. J Orthop Trauma 13(3):178–186
13. Schütz M, Südkamp NP (2003) Revolution in plate osteosynthesis: new internal fixator systems. J Orthop Sci 8(2):252–258
14. Taljanovic MS, Hunter TB, Miller MD, Sheppard JE (2005) Gallery of medical devices: part 1: orthopedic devices for the extremities and pelvis. Radiographics 25(3):859–870

15. Malekani J, Schmutz B, Gu Y, Schuetz M, Yarlagadda P (2017) Orthopedic bone plates: evolution in structure, implementation technique and biomaterial. GSTF J Eng Technol (JET) 1(1):135–140
16. Chakladar N, Harper LT, Parsons A (2016) Optimisation of composite bone plates for ulnar transverse fractures. J Mech Behav Biomed Mater 57:334–346
17. Sanjairaj V, Kannan S, Cao T, Fuh JYH, Sriram G, Lu WF (2019) 3D-printed PCL/PPy conductive scaffolds as three-dimensional porous nerve guide conduits (NGCs) for peripheral nerve injury repair. Front Bioeng Biotechnol 7:266
18. Vijayavenkataraman S, Vialli N, Fuh JY, Lu WF (2019) Conductive collagen/PPy-b-PCL hydrogel for bioprinting of neural tissue constructs. Int J Bioprint 5(2.1):229
19. Navarro M, Michiardi A, Castano O, Planell J (2008) Biomaterials in orthopaedics. J R Soc Interface 5(27):1137–1158
20. Zhang S, Vijayavenkataraman S, Chong GL, Fuh JYH, Lu WF (2019) Computational design and optimization of nerve guidance conduits for improved mechanical properties and permeability. J Biomech Eng Trans ASME 141(5):051007
21. Balla VK, Bose S, Davies NM, Bandyopadhyay A (2010) Tantalum—a bioactive metal for implants. JOM 62(7):61–64
22. Vijayavenkataraman S, Zhang L, Zhang S, Hsi Fuh JY, Lu WF (2018) Triply Periodic minimal surfaces sheet scaffolds for tissue engineering applications: an optimization approach toward biomimetic scaffold design. ACS Appl Bio Mater 1(2):259–269
23. Pobloth A-M, Checa S, Razi H, Petersen A, Weaver JC, Schmidt-Bleek K, Windolf M, Tatai AÁ, Roth CP, Schaser K-D (2018) Mechanobiologically optimized 3D titanium-mesh scaffolds enhance bone regeneration in critical segmental defects in sheep. Sci Transl Med. https://doi.org/10.1126/scitranslmed.aam8828
24. Park I-P, Heo S-J, Koak J-Y, Kim S-K (2010) Post traumatic malocclusion and its prosthetic treatment. J Adv Prosthodont 2(3):88–91
25. Cervantes TM, Slocum AH Jr, Seldin EB (2012) Design and experimental evaluation of adjustable bone plates for mandibular fracture fixation. J Biomech 45(1):172–178
26. Munib Z, Ali MN, Ansari U, Mir M (2015) Auxetic polymeric bone stent for tubular fractures: design, fabrication and structural analysis. Polym Plast Technol Eng 54(16):1667–1678
27. Kolken HM, Janbaz S, Leeflang SM, Lietaert K, Weinans HH, Zadpoor AA (2018) Rationally designed meta-implants: a combination of auxetic and conventional meta-biomaterials. Mater Horiz 5(1):28–35
28. Mehmood S, Ali MN, Ansari U, Mir M, Khan MA (2015) Auxetic polymeric bone plate as internal fixator for long bone fractures: design, fabrication and structural analysis. Technol Health Care 23(6):819–833
29. Kolken HM, Zadpoor A (2017) Auxetic mechanical metamaterials. RSC Advances 7(9):5111–5129
30. Yang D, Lee S, Huang F (2003) Geometric effects on micropolar elastic honeycomb structure with negative Poisson's ratio using the finite element method. Finite Elem Anal Design 39(3):187–205
31. Gaspar N, Ren X, Smith CW, Grima J, Evans KE (2005) Novel honeycombs with auxetic behaviour. Acta Mater 53(8):2439–2445
32. Veronda D, Westmann R (1970) Mechanical characterization of skin—finite deformations. J Biomech 3(1):111–124
33. Lees CV (1991) JE Poisson's ratio in skin. Biomed Mater Eng 1:1
34. Williams J, Lewis J (1982) Properties and an anisotropic model of cancellous bone from the proximal tibial epiphysis. J Biomech Eng 104(1):50–56
35. Soman P, Fozdar DY, Lee JW, Phadke A, Varghese S, Chen S (2012) A three-dimensional polymer scaffolding material exhibiting a zero Poisson's ratio. Soft Matter 8(18):4946–4951
36. Vijayavenkataraman S, Thaharah S, Zhang S, Lu WF, Fuh JYH (2019) 3D-printed PCL/rGO conductive scaffolds for peripheral nerve injury repair. Artif Organs 43(5):515–523